Some Modes of the Incompressible Flow on an Elliptic Cylinder at Low Reynolds Number

M. Boubekri and M. Afrid

Department of Physics, University of Mentouri, 25000 Constantine, Algeria

Abstract: We consider the numerical simulation of the two-dimensional viscous flow over a solid ellipse with an aspect ratio equal 3.5. Sufficiently far from the ellipse, the flow is assured potential. The flow is modelled by the two dimensional partial differential equations of conservation of masse and moment, using elliptic coordinates. The finite volume method is used to discritize the model equations. The numerical solutions revealed that the flow over the ellipse is steady with zero vortex up to Re = 40. For Reynolds numbers between 50 and 190, the flow is steady with two vortices in the wake. For Re = 210 the flow becomes unstable with harmonic oscillations: The two vortices are alternate in the time with a Strouhal number equal to 0.2075. For the Reynolds number between 220 and 280 the vortices are detached one after other. The spectral analysis of the discrete time variation of the flow velocity at a point within the upper vortex shows that the dominant oscillations frequency is f = 0.2748.

Key words: Elliptic cylinder, finite volumes, wake, vortex, Reynolds number

INTRODUCTION

There have been many experimental and numerical studies of fluid flow from elliptical cylinders. Schubauer (1939) studied experimentally the distribution of velocity in the laminar boundary layer on the surface of an elliptic cylinder with axes ratio equal to 3. He found that the velocity distribution in the boundary layer, its thickness, and its separation from the surface of the body depend entirely on the velocity distribution in the region of potential flow, outside the boundary layer. Yano and Kieda (1980) presents an approximate method for solving Ossen's linearized equations for two-dimensional steady flow of incompressible viscous fluid past an inclined elliptic cylinder at low Reynolds numbers. Aspect Ratio is AR = 0.1 and 0.5. The Reynolds number varied between 0.01 and 5. Angle of attack is: $\alpha = 0°$, 45 and 90°. The drag and lift coefficients have maximum values at $\alpha = 90°$ and $\alpha = 45°$, respectively. Mittal and Balachandar (1996) conducted two and three dimensional simulations of an incompressible viscous flow over elliptic cylinders. They used spectral methods. The ellipse aspect ratio is AR = 2 and the span wise aspect ratio A = 2. Two angles of attack 0 and 45° were considered. The Reynolds number is fixed to 525. The drag coefficient calculated with the three-dimensional simulation agrees better with the experimental value than that of the two-dimensional simulation. The values of the coefficient of drag obtained with the two-dimensional simulation are 74, 16 and 1.3%

higher than those obtained with the three-dimensional simulation. Allessio and Kocabiyik (2001) studied numerically the flow of a viscous incompressible fluid past an inclined elliptic cylinder which starts translating and oscillating impulsively. These oscillations are allowed in a direction perpendicular to the uniform oncoming flow having a magnitude which is less than or equal to the constant translational velocity. The investigation is based on an implicit finite difference/spectral scheme for integrating the unsteady Navier-Stokes equations expressed in a stream function/vorticity formulation. The Reynolds number is fixed to Re = 10^3. Two angles of attack $\alpha = 45°$ and $\alpha = 90°$ were considered. They examine the effect of increase of velocity ratio on the near-wake structure as well as the hydrodynamic forces acting on the cylinder. Vortex dynamics close behind the cylinder are affected by the changing acceleration of the cylinder. An interesting phenomenon has been observed in the flow patterns depending on the velocity ratio and the angle of inclination. In all cases considered in this study, the C_L curve oscillates with the forcing frequency of the cylinder whereas a switch over in the nature of the fluctuations of the drag coefficient is observed with the increase of angle of inclination. Choi and Lee (2001) studied experimentally the flow characteristics around an elliptic cylinder with axes ratio of AR = 2 located near a flat plate. The Reynolds numbers Based on the height (B) of the elliptic cylinder and the boundary layer thickness (δ) were $Re_B = 13600$ and $Re_\delta = 48000$, respectively. Tree

---

Corresponding Author: M. Boubekri, Department of Physics, University of Mentouri, 25000 Constantine, Algeria

angles of attack: -5, 0 and +5° were considered in order to study the interaction between the cylinder wake and the boundary layer. As the angle of attack varies, the location of the peak pressure on the windward cylinder surface moves towards the rear edge of the cylinder, while that of the leeward surface moves toward the front edge of the cylinder. At positive angles of attack, the location of the minimum surface pressure on the flat plate moves downstream slightly, whereas it moves upstream for negative angles of attack. Johnson *et al.* (2001) studied numerically the flow around an elliptical cylinder with varying aspect ratios and Reynolds numbers. They used spectral methods. The aspect ratios ranging from 0.01 to 1.00 and for Reynolds numbers ranging from 30-200. Six different types of flow patterns were categorized in the simulations. These were, steady flow, Von Karman-type vortex shedding, symmetric wake, transitional vortex shedding, steady secondary shedding and unsteady secondary shedding. They have shown substantial change in the shedding types caused by the convective instability interacting with the vortex shedding occurring behind the cylinder. Khan *et al.* (2004) studied analytically heat transfer and flow around elliptical cylinder in the Reynolds number range of 10^2 to 10^5. The ellipse aspect ratio is AR = 2, 3 and 4. Three general correlations, one for the drag coefficient and two for the heat transfer under each thermal boundary condition, have been determined. It is observed that the drag coefficients are lower whereas the average heat transfer coefficients are higher for elliptical cylinders than for circular cylinder. In this study, we consider the two-dimensional numerical simulation of the incompressible flow around an elliptic cylinder. The ellipse axes ratio is fixed to 3.5 and the flow far away from the solid ellipse (outer boundary condition) is assumed potential. The Reynolds number is varied from 10-280.

MATHEMATICAL MODEL

The transformation equations from the elliptic coordinates to the Cartesian coordinates are:

$$\begin{aligned} x &= a\cosh(\varepsilon)\cos(\eta) \\ y &= a\sinh(\varepsilon)\sin(\eta) \end{aligned} \tag{1}$$

Where, a is the distance between the center and the foci of the ellipse. Lines of constant ε correspond to confocal ellipses and lines of constant η correspond to hyperbolas. The metrics of the transformation are:

$$h_1 = h_2 = a\sqrt{\sinh^2(\varepsilon) + \sin^2(\eta)} \tag{2}$$

The Jacobian of the transformation is:

$$J(\varepsilon, \eta) = h_1 h_2 \tag{3}$$

The flow around the ellipse is modelled by the conservation partial differential equations of mass and momenta (Navier-Stokes equations), with their initial and boundary conditions. The non dimensional model equations are written in the elliptic coordinates system: The initial conditions:

At t = 0,

$$V_\varepsilon = V_\eta = P = 0 \tag{4}$$

For t > 0

The equation of continuity:

$$\frac{1}{h_1 h_2}\frac{\partial}{\partial \varepsilon}\left(h_2 V_\varepsilon\right) + \frac{1}{h_1 h_2}\frac{\partial}{\partial \eta}\left(h_1 V_\eta\right) = 0 \tag{5}$$

The momentum equation in the ε direction:

$$\begin{aligned} &\frac{\partial V_\varepsilon}{\partial t} + \frac{1}{h_1 h_2}\frac{\partial\left(h_2 V_\varepsilon V_\varepsilon\right)}{\partial \varepsilon} + \frac{1}{h_1 h_2}\frac{\partial\left(h_1 V_\eta V_\varepsilon\right)}{\partial \eta} \\ &-\frac{1}{h_1 h_2}V_\eta^2\frac{\partial h_2}{\partial \varepsilon} + \frac{1}{h_1 h_2}V_\eta V_\varepsilon\frac{\partial h_1}{\partial \eta} = \\ &\left[\begin{array}{l}\frac{2}{h_1 h_2}\frac{\partial}{\partial \varepsilon}\left(\frac{\partial V_\varepsilon}{\partial \varepsilon}\right) + \frac{1}{h_1 h_2}\frac{\partial}{\partial \eta}\left(\frac{\partial V_\varepsilon}{\partial \eta}\right) - \\ \frac{1}{h_1 h_2}\frac{\partial}{\partial \eta}\left(\frac{V_\varepsilon}{h_1}\frac{\partial h_1}{\partial \eta}\right) + \frac{2}{h_1 h_2}\frac{\partial}{\partial \varepsilon}\left(\frac{V_\eta}{h_1}\frac{\partial h_1}{\partial \eta}\right) \end{array}\right] \\ &-\frac{1}{h_1}\frac{\partial P}{\partial \varepsilon} + \frac{1}{Re}\left[\begin{array}{l}+\frac{1}{h_1 h_2}\frac{\partial}{\partial \eta}\left(h_1\frac{\partial}{\partial \varepsilon}\left(\frac{V_\eta}{h_2}\right)\right) + \frac{1}{h_1 h_2} \\ \left(\frac{\partial}{\partial \varepsilon}\left(\frac{V_\eta}{h_2}\right) + \frac{\partial}{\partial \eta}\left(\frac{V_\eta}{h_1}\right)\right)\frac{\partial h_1}{\partial \eta} \\ -\frac{2}{h_1 h_2}\left(\frac{1}{h_1}\frac{\partial V_\eta}{\partial \eta} + \frac{V_\varepsilon}{h_1 h_2}\frac{\partial h_2}{\partial \varepsilon}\right)\frac{\partial h_2}{\partial \varepsilon}\end{array}\right] \end{aligned} \tag{6}$$

The momentum equation in the η direction:

$$\begin{aligned} &\frac{\partial V_\eta}{\partial t} + \frac{1}{h_1 h_2}\frac{\partial\left(h_2 V_\varepsilon V_\eta\right)}{\partial \varepsilon} + \frac{1}{h_1 h_2}\frac{\partial\left(h_1 V_\eta V_\eta\right)}{\partial \eta} \\ &-\frac{1}{h_1 h_2}V_\varepsilon^2\frac{\partial h_1}{\partial \eta} + \frac{1}{h_1 h_2}V_\eta V_\varepsilon\frac{\partial h_2}{\partial \varepsilon} = \\ &\left[\begin{array}{l}\frac{1}{h_1 h_2}\frac{\partial}{\partial \varepsilon}\left(\frac{\partial V_\eta}{\partial \varepsilon}\right) + \frac{2}{h_1 h_2}\frac{\partial}{\partial \eta}\left(\frac{\partial V_\eta}{\partial \eta}\right) - \\ \frac{1}{h_1 h_2}\frac{\partial}{\partial \varepsilon}\left(\frac{V_\eta}{h_2^*}\frac{\partial h_2}{\partial \varepsilon}\right) + \frac{2}{h_1 h_2}\frac{\partial}{\partial \eta}\left(\frac{V_\varepsilon}{h_2}\frac{\partial h_2}{\partial \varepsilon}\right) \end{array}\right] \\ &-\frac{1}{h_2}\frac{\partial P}{\partial \eta} + \frac{1}{Re}\left[\begin{array}{l}+\frac{1}{h_1 h_2}\frac{\partial}{\partial \varepsilon}\left(h_2\frac{\partial}{\partial \eta}\left(\frac{V_\varepsilon}{h_1}\right)\right) + \frac{1}{h_1 h_2} \\ \left(\frac{\partial}{\partial \varepsilon}\left(\frac{V_\eta}{h_2}\right) + \frac{\partial}{\partial \eta}\left(\frac{V_\varepsilon}{h_1}\right)\right)\frac{\partial h_2}{\partial \varepsilon} \\ -\frac{2}{h_1 h_2}\left(\frac{1}{h_1}\frac{\partial V_\varepsilon}{\partial \varepsilon} + \frac{V_\eta}{h_1 h_2}\frac{\partial h_1}{\partial \eta}\right)\frac{\partial h_1}{\partial \eta}\end{array}\right] \end{aligned} \tag{7}$$

The model equations are solved with the following boundary conditions:

At the surface of the ellipse: $c = c_i = 0.2939$:

$$V_z = V_\eta = 0 \qquad (8)$$

At the outer boundary of the domain according to Gontier (1969), the flow is assumed is potential and hence:

At $c = c_e = 3$

$$V_z = \frac{1}{h_1}\left[1 - \frac{\lambda(\varepsilon)}{\lambda(\varepsilon_i)}\right]\sinh(\varepsilon)\,\cos(\eta)$$

$$V_\eta = -\frac{1}{h_2}\left[1 + \frac{\mu(\varepsilon)}{\lambda(\varepsilon_i)}\right]\cosh(\varepsilon)\,\sin(\eta) \qquad (9)$$

With:

$$\lambda(\varepsilon) = \frac{\cosh(\varepsilon)}{\sinh^2(\varepsilon)} + \ln\left(\tanh\left(\frac{\varepsilon}{2}\right)\right)$$

$$\mu(\varepsilon) = -\frac{1}{\cosh(\varepsilon)}\left[1 + \cosh(\varepsilon)\cdot\ln\left(\tanh\left(\frac{\varepsilon}{2}\right)\right)\right] \qquad (10)$$

NUMERICAL DISCRETIZATION AND SOLUTION

This study, we use the finite volume method to descretize the model equations. The time derivative terms are descretized as follows:

$$\frac{\partial\phi}{\partial t} = \frac{3\phi^{t+\Delta t} - 4\phi^t + \phi^{t-\Delta t}}{2\Delta t}$$

All the convective and non linear terms as well as the diffusive terms (except the first and the second on the right of Eq. 6 and 7) are temporally descretized with the Adam-Bashforth second accurate scheme:

$$\phi^{t+\Delta t} = 2\phi^t - \phi^{t-\Delta t}$$

This second order discretization is that of Adam-Bashforth. The pressure terms and the first two diffusive terms on the right of Eq. 6 and 7 are implicit that means they are evaluated at time $(t + \Delta t)$.

We use the central difference spatial discretization which is second order accurate. Thus, the numerical discretization of this study is second order accurate in space and time: the truncation error is of second order. A discretization equation is obtained by the multiplication of the differential equation by the differential volume $J (c, \eta)\, dc\, d\eta$ and the double integration between the limits of the considered finite volume. The details of the discretization of the model equations, with the method of finite volumes, are similar to those presented by Patankar (1980) for the Cartesian case. However, in this study, the discretization is second order accurate whereas that of the mentioned reference is first order accurate. Each discretization equation has the form:

$$A_P\,\Phi_P^{t+\Delta t} = A_N\,\Phi_N^{t+\Delta t} + A_S\,\Phi_S^{t+\Delta t} + A_E\,\Phi_E^{t+\Delta t} + A_W\,\Phi_W^{t+\Delta t} + S$$

The sequential solution of the systems of discretization equations follows the Simpler algorithm (Patankar, 1980). The linear systems of discretization equations are solved by the method of sweeping using the algorithm of Thomas and the tri diagonal cyclic algorithm. A 62×142 uniform grid is used. From the initial conditions, time marching is continued with the time step $\Delta t = 10^{-3}$ until a steady state solution is obtained or an established transient flow is obtained.

RESULTS

In Fig. 1, we present the pressure field and the streamlines of the flow obtained with Re = 10. This flow is steady. The pressure field is symmetric with respect to the horizontal axis. The maximum pressure is located on the ellipse leading edge. Between the leading edge and the trailing edge, the pressure decreases continuously.

For Reynolds numbers between 50 and 200, we obtained a flow with two vortices (Fig. 2). This flow is also steady and symmetric with respect to the horizontal line. On the ellipse, the points of separation for Re = 170 are $\eta = 0.612$ and $\eta = 5.668$. We observe two fixed contra rotating vortices between the points of separation and the downstream of the trailing edge. The size of the vortex grows as the Reynolds number increases. On the ellipse
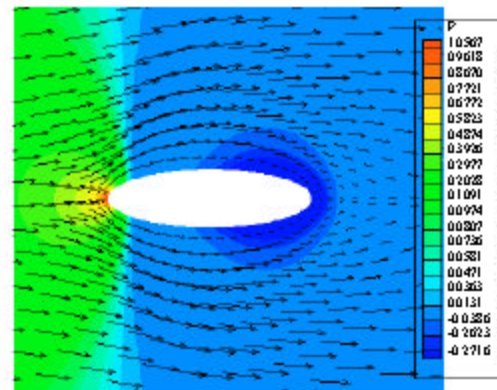

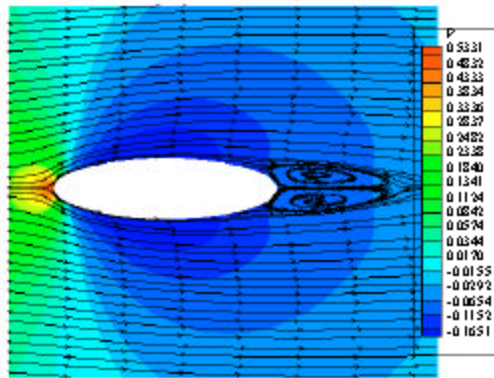Fig. 1: The field of pressure and linens of current for Re = 10

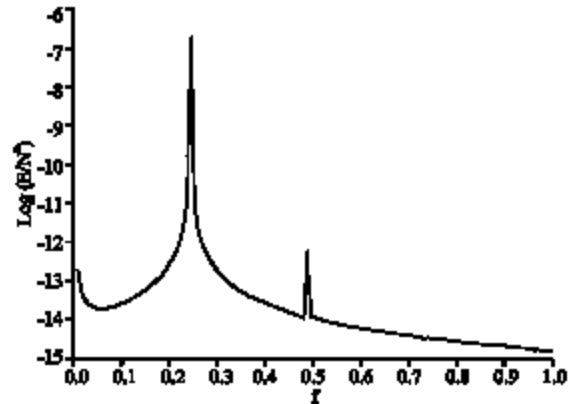Fig. 2: The pressure field and streamlines for Re = 170

Fig. 4: The spectrum of energy for Re = 210
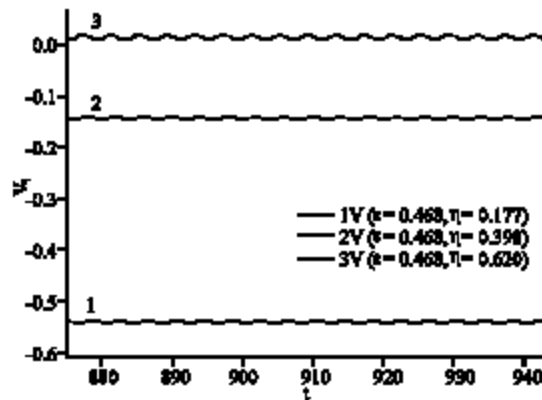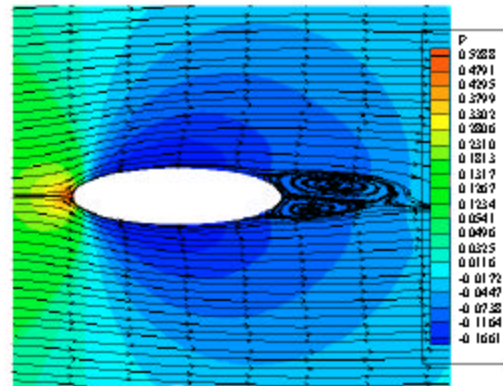

Fig. 3: Temporal variation of velocity for Re = 210

Fig. 5: The pressure field and streamlines for Re = 210

surface, the maximum pressure is at the leading edge, it decreases downstream up to the point $\eta = 1.499$ on the upper surface and $\eta = 4.79$ on the lower surface. From these points to the trailing edge the pressure increases slightly.

For the Reynolds number equal to 210 the flow becomes unstable: oscillatory and harmonic. In Fig. 3, we record the time oscillations velocity at three locations: $(c = 0.468, \eta = 0.177), (c = 0.468, \eta = 0.398)$ and $(c = 0.468, \eta = 0.620)$. To make sure that the temporal oscillations of the flow are physical and not numerical, we reduced the step from to $\Delta t = 10^{-3}$ to $\Delta t = 5.10^{-4}$ we obtained the same oscillations (with the same amplitude and frequency). The spectral analysis of the velocity time oscillations V_η $(c = 0.468, \eta = 0.620)$ has shown that the frequency is $f = 0.2075$ (Fig. 4).

In Fig. 5, we represent the field of pressure and the streamlines of the flow. It is noticed that the flow is asymmetrical in the zone of the wake compared to the

horizontal axis of the ellipse. The two vortexes are of different size. The maximum pressure is located at the edge of attack and decreases gradually on the surface of the ellipse up to the points: $\eta = 1.555$ on the upper surface and $\eta = 4.577$ on lower surface.

When the Reynolds number is varied between 220 and 280, the flow remains unsteady with harmonic oscillatory. In Fig. 6, we recorded the time oscillations of the velocity at three locations: $(c = 0.468, \eta = 0.177)$, $(c = 0.468, \eta = 0.398)$ and $(c = 0.468, \eta = 0.620)$. To make sure that the temporal oscillations of the flow are physical and not numerical, we reduce the step from $\Delta t = 10^{-3}$ to $\Delta t = 5.10^{-4}$ and we obtained the same oscillations (with the same amplitude and frequency). The spectral analysis of the velocity time oscillations of the velocity V_η $(c = 0.468, \eta = 0.177)$ has shown that the frequency is $f = 0.2748$ (Fig. 7).

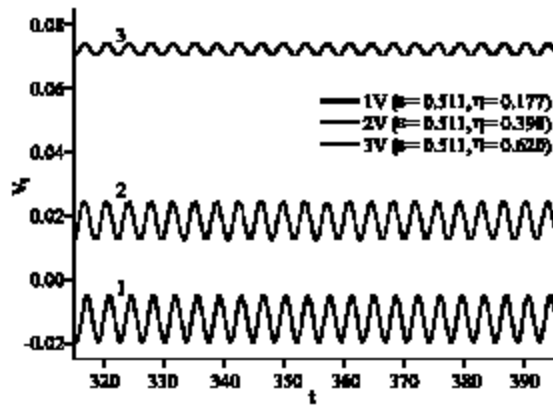In Fig. 8, we illustrate the pressure field and the streamlines of the flow obtained with Re = 280 at the time
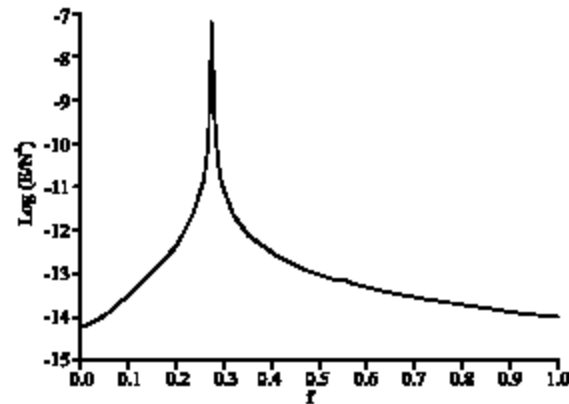
Fig. 6: Temporal variation of velocity for Re = 280
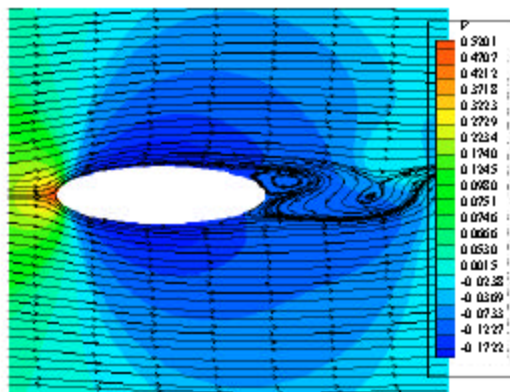

Fig. 7: The spectrum of energy for Re = 280

Fig. 8: The pressure field and streamlines for Re = 280

t = 404. It is noticed that the flow in the zone of the wake is asymmetric with respect to the horizontal axis of the ellipse. The two vortices close to the trailing edge have different sizes: the upper vortex is larger. The maximum pressure is at the leading edge. Along the surface of the ellipse, the pressure falls staring from the leading edge up
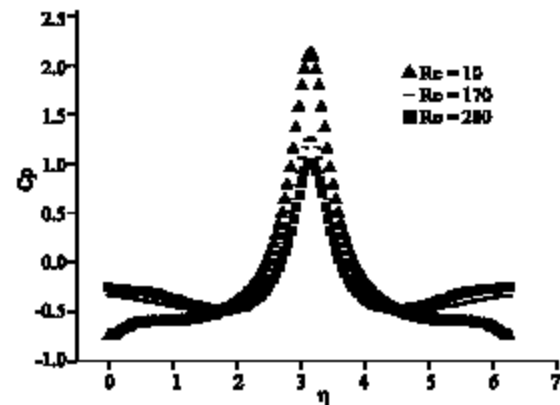

Fig. 9: Variation of pressure coefficient with the Reynolds number

to η = 1.555 on the upper surface and η = 4.577 on the lower surface. From these points to the trailing edge the pressure increases slightly (Fig. 9).

CONCLUSION

In this study, we considered the numerical simulation of the incompressible two-dimensional external flow over an elliptic cylinder. We fixed the aspect ratio AR = 3.5 and we varied the Reynolds numbers between 10 and 280. We found 3 flow regimes. For Reynolds numbers between 10 and 40, we found a flow with no vortices. For Reynolds numbers between 50 and 200 we obtained a flow with two vortices attached to rear of the elliptic cylinder. For Re = 210 the flow becomes unstable with harmonic oscillations: The two vortices are alternate in the time with a Strouhal number equal to 0.2075. For Reynolds numbers between 220 and 280, the flow bifurcates to an oscillatory harmonic regime with a frequency f = 0.2748.

REFERENCES

Allessio, S.J.D.D. and S. Kocabiyik, 2001. Numerical simulation of the flow induced by a transversely oscillating inclined elliptic cylinder. J. Fluids Struct., 15: 691-715.

Choi, J.H. and S.J. Lee, 2001. flow characteristics around an inclined elliptic cylinder in a turbulent boundary layer. J. Fluids Struct., 15: 1123-1135.

Gontier, G., 1969. Mécanique des milieux déform-ables. DUNOD, Paris.

Johnson, S.A. M.C. Thompson and K. Hourigan, 2001. Flow past Elliptical Cylinders at Low Reynolds Numbers. 14th Australasian Fluid Mechanics Conference Adelaide University, Adelaide, Australia.

Khan, W.A., J.R. Culham and M.M. Yovanovich, 2004. Fluid flow and heat transfer from elliptical cylinders: Analytical approach. 37th AIAA Thermophysics Conference Portland.

Mittal, R. and S. Balachander, 1996. Direct Numerical Simulation of Flow Past Elliptic Cylinders. J. Computational Phys., 124: 351-367.

Patankar, S., 1980. Numerical Heat Transfer and Fluid Flow. McGraw-Hill Book Company.

Schubauer, G.B., 1939. Air Flow in the boundary layer of an elliptic cylinder. T.R. No 652, N.A.C.A.

Yano, H. and A. Kieda, 1980. An approximate method for solving two-dimensional low-Reynolds-number flow past arbitrary cylindrical bodies. J. Fluid Mech., 97: 157-159.